



Journal of Mining and Environment (JME)

journal homepage: [www.jme.shahroodut.ac.ir](http://www.jme.shahroodut.ac.ir)



## Numerical Investigation of Effect of Rock Bolt Angle on Shear Behavior of Rock Bridges

Vahab Sarfarazi<sup>1\*</sup> and Abdollah Tabaroei<sup>2</sup>

1. Department of Mining Engineering, Hamedan University of Technology, Hamedan, Iran

2. Department of Civil Engineering, Eshragh Institute of Higher Education, Bojnourd, Iran

### Article Info

Received 18 April 2020

Received in Revised form 10 September 2020

Accepted 1 October 2020

Published online 5 October 2020

DOI: [10.22044/jme.2020.9580.1871](https://doi.org/10.22044/jme.2020.9580.1871)

### Keywords

Rock Bridge

Rock Bolt

PFC2D

### Abstract

In this work, the effect of rock bolt angle on the shear behavior of Rock Bridges is investigated using the particle flow code in two dimensions (PFC2D) for three different Rock Bridge lengths. Firstly, the calibration of PF2D is performed to reproduce the gypsum sample. Then the numerical models with the dimensions of 100 mm \* 100 mm are prepared. The Rock Bridge is created in the middle of the model by removal of the narrow bands of discs from it. The uniaxial compressive strength of the Rock Bridge is 7.4 MPa. The Rock Bridge lengths are 30 mm, 50 mm, and 70 mm. The rock bolt is calibrated by a parallel bond. The tensile strength of the simulated rock bolt is 360 MPa. One rock bolt is implemented in the Rock Bridge. The rock bolt angles related to the horizontal axis are the changes from 0 to 75 degrees. Totally, 18 models are prepared. The shear test condition is added to the models. The normal stress is fixed at 2 MPa, and the shear load is added to the model till failure occurs. The results obtained show that in a fixed rock bolt angle, the tensile crack initiates from the joint tip and propagates parallel to the shear loading axis till coalescence to rock bolt. In a constant Rock Bridge length, the shear strength decreases with increase in the rock bolt angle. The highest shear strength occurs when the rock bolt angle is 0°.

### 1. Introduction

The Rock Bridges and the joints that are extremely common in rock masses, and the stability of a jointed rock mass mostly depend on the mechanical properties of the joints and Rock Bridges. Since the 1960s, the shear behavior of rock joints has been the focus of many studies, and many achievements have been made [1–10]. The results of the previous research works have shown that the parameters such as the joint asperity, joint surface strength, degradation, filling and dip and dip direction have important effects on the shear strength of the joint surface. Rock bolts have been widely used in engineering due to their convenience, affordability, and reliability. However, the anchoring mechanism for a jointed rock mass is still not clearly understood. As it is known, the anchoring mechanism for a bolted rock mass is highly complex due to the anisotropy of the rock mass and the complexity of the joint pattern.

Many scholars have conducted experimental and theoretical studies in order to reveal the anchoring mechanism in a bolted rock joint. Spang and Egger [11] have conducted a series of shear tests on a bolted joint to study the deformation characteristics of a bolt, and have found two critical points in a bolt: one at the bolt-joint intersection and the other at the hinge point. Egger and Zabuski [12] have found that the anchoring mechanism of a bolt in a reinforced joint contributes an additional shear resistance to prevent the shear failure of a joint. Bolt deformation typically occurs near the joint. Ferrero [13] has proposed a shear strength model for a reinforced joint that consider both the dowel effect and the incremental increase in the axial force due to the bar deformation. Pellet and Egger [14] have related the theoretical and experimental analyses of the rock bolt shear strength, and have found that the bolts installed perpendicular to a

Corresponding author: [vahab.sarfarazi@gmail.com](mailto:vahab.sarfarazi@gmail.com) (V. Sarfarazi).

joint plane allow the greatest displacement along a joint prior to failure but the displacement at failure decrease rapidly as the angle between the bolt and the joint plane decreases. Jalalifar and Aziz [15] have performed double shear tests and numerical simulations on five types of bolts in order to study the bolt force and failure mechanism. Wang et al. [16] have used ANSYS to calculate the stress intensity factors on the tip of cracks for different anchoring conditions, obtaining a relationship between the anchoring spacing, anchoring angle, and stress intensity factor using the FLAC3D software to simulate the coalescence modes for main-control cracks at different anchor spacing. Li et al. [17] have analyzed a numerical model of a fully grouted rock bolt installed in concrete with FLAC3D, and have concluded that the bolt's resistance to shear is influenced by the rock strength, inclination angle, and diameter of the rock bolt. In the recent years, with the development of high-power computers, the numerical software particle flow code (PFC) based on the discrete element method has become increasingly mature in studying the rock and soil failure behavior [18]. Many achievements have been made in determining the mechanical properties of rock joints [19–23]. Rock joints effectively compensate for the lack of repeatable rock mass. Some studies have examined the roughness of jointed rock mass using a DEM model. For example, Xia et al. [24] have carried out a numerical simulation of shear experiments on non-bolted rock using the discrete element software PFC2D, and have analyzed the direct shear characteristics of rough joints. Using the experimental results of rock joints, Zhou et al. [25] have analyzed the fracture evolution characteristics of a rock mass during shearing via the discrete element PFC software. Cao et al. [26] have used PFC in order to generate shear models with different roughness values, and have discussed the influence of roughness on the surface morphology of non-anchor joints from a micro viewpoint.

In this work, the effect of rock bolt angle on the shear behavior of Rock Bridges was investigated

using PFC in two dimensions for three different Rock Bridge lengths.

## 2. Materials and Methods

### 2.1. PFC Software

PFC is a discrete element commercial software developed by the Itasca Consulting Group, and has already been widely used in the rock mechanics field [18]. PFC2D represents a rock mass as an assemblage of circular disks with a finite thickness connected via the cohesive and frictional bonds. A basic linear contact model describes the elastic relationship between the relative displacements and forces of disks at the point contact, as shown in Figure 1. This model involves the contact normal force component,  $F_n$ , contact overlap,  $U_n$ , shear force increment,  $\Delta F_s$ , and shear displacement increment,  $\Delta U_s$ , and is given by:

$$F_n = k_n U_n \quad (1)$$

where  $kn$  is the normal stiffness at the contact. The value of  $kn$  is determined by the current contact stiffness model. Note that the normal stiffness,  $kn$ , is a secant modulus in that it relates the total displacement and force. The shear stiffness,  $ks$ , on the other hand, is a tangent modulus in that it relates the incremental displacement and force. An upper case  $K$  is used to denote a secant modulus, and a lower case  $k$  is used to denote a tangent modulus. The computation of the normal contact force from the geometry alone makes the code less prone to numerical drift, and is able to handle arbitrary placement of balls and changes in ball radii after a simulation has begun. The shear contact force is computed in an incremental fashion. When the contact is formed, the total shear contact force is initialized to zero. Each subsequent relative shear displacement increment results in an increment of elastic shear force that is added to the current value. The motion of the contact must be considered during this procedure.

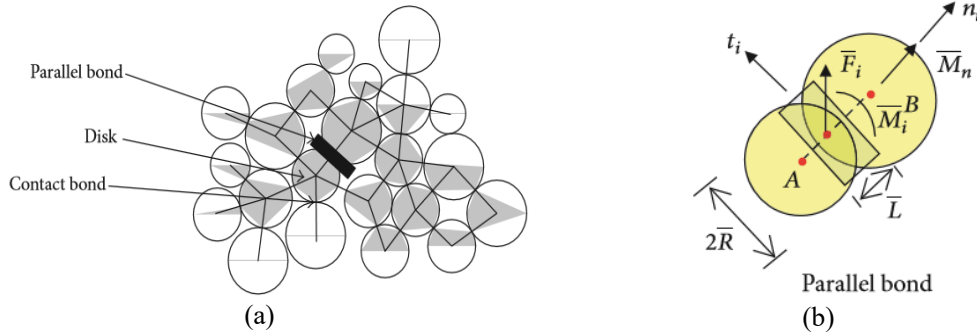


Figure 1. Parallel bond model and stress state between disks [18].

The contact velocity can be resolved into the normal and shear components with respect to the contact plane. Denoting these components by  $V_i^n$  and  $V_i^s$  for the normal and shear components, respectively, the shear component of the contact velocity can be written as:

$$V_i^s = V_i - V_i^n n_i n_i \quad (2)$$

The shear component of the contact displacement increment vector occurring over a time step of  $\Delta t$  is calculated by:

$$\Delta U_i^s = V_i^s \Delta t \quad (3)$$

and is used to calculate the shear elastic force-increment vector:

$$\Delta F_s = -k_s \Delta U_s \quad (4)$$

The frictional resistance of the contact is given by:

$$F_s \leq \mu F_n \quad (5)$$

where  $\mu$  is the friction coefficient between the disks. In order to simulate a relatively brittle rock-like material, it is necessary to cement these disks with a bonded model. This work uses the parallel bond model, which resists not only the contact forces but also the moments between the disks at a cemented contact (Figure 1). The strength of the cemented contact is then given by:

$$\begin{aligned} \bar{\sigma}_{\max} &= \frac{-\bar{F}_n}{A} + \frac{|\bar{M}_s| \bar{R}}{I} < \bar{\sigma}_c \\ \bar{\tau}_{\max} &= \frac{-\bar{F}_s}{A} + \frac{|\bar{M}_n| \bar{R}}{J} < \bar{\tau}_c \end{aligned} \quad (6)$$

where  $\bar{R}$  is the radius of the bonded zone between the disks,  $t$  is the length of the bonded zone

between the disks (Figure 1), and  $\bar{\sigma}_c$  and  $\bar{\tau}_c$  are the tensile and shear strength of the bond contact, respectively. The tensile cracks occur when the applied tensile stress exceeds the specified tensile strength of the parallel bond,  $\bar{\sigma}_c$ . The shear cracks occur when the applied shear stress exceeds the specified shear strength of the parallel bond,  $\bar{\tau}_c$ , either by rotation or by shearing of the disks. The tensile strength at the contact immediately drops to zero once the crack occurs, and the shear strength reduces to the residual friction strength (Itasca Consulting Group Inc. [18], Potyondy [21]), as illustrated in Figure 2.

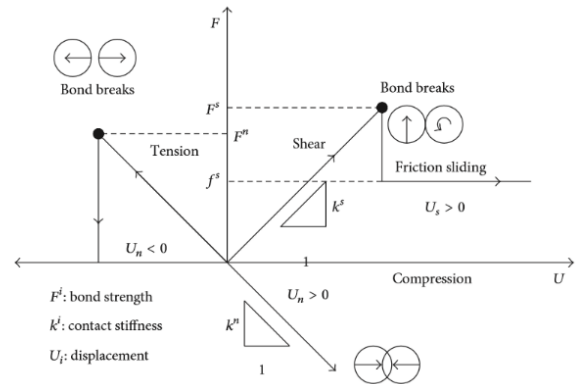


Figure 2. Illustration of the yield process for a parallel bond, Potyondy [22].

## 2.2. Direct Shear Simulation of Bolted Joint using PFC

### 2.2.1. Micro parameters of gypsum sample or material condition

The standard process of generating a PFC2D assembly to represent a gypsum model used in this work has been described in detail by Potyondy and Cundall [21]. The process involves particle generation, packing the particles, isotropic stress installation (stress initialization), floating particle (floater) elimination, and bond installation. A gravity effect was not required to be considered as

the specimens were small, and the gravity-induced stress gradient had a negligible effect on the macroscopic behavior. The uniaxial compressive strength and the Brazilian tests were carried out to calibrate the properties of the particles and parallel bonds in the bonded particle model (Ghazvinian *et al.* [27]). Adopting the micro-properties listed in Table 1 and the standard calibration procedures (Potyondy and Cundall [21]), a calibrated PFC particle assembly was created. Figures 3a and 3b show the experimental uniaxial compression test and the numerical simulation, respectively. Also

Figures 3c and 3d show the experimental Brazilian test and the numerical simulation, respectively. The results obtained show a well matching between the experimental test and the numerical simulation. Table 2 shows a comparison between the mechanical properties rendered by the experimental test and the numerical simulation. The results show a well matching between the experimental test and the numerical simulation. It is to be noted that E modulus is generally more than UCS. This result was gained from the experimental test.

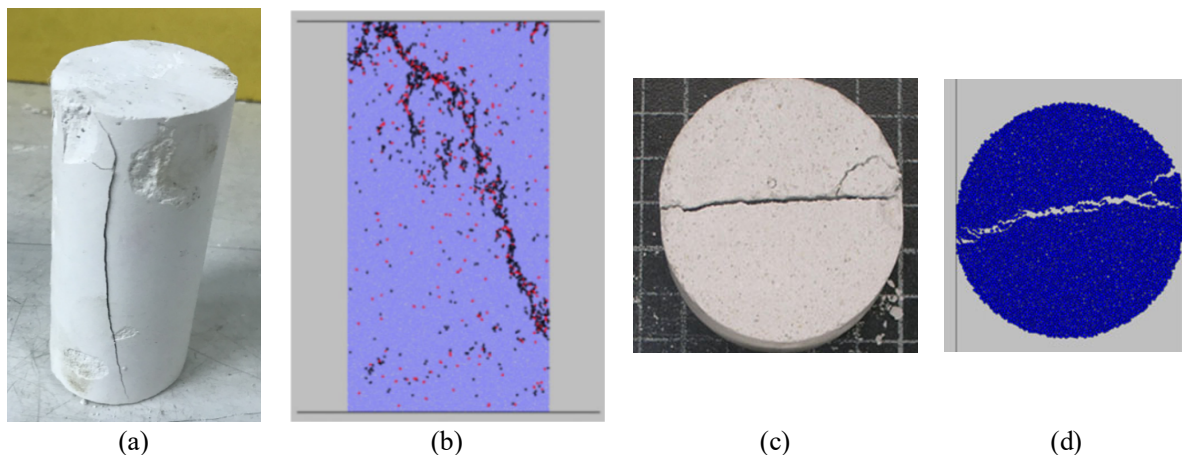


Figure 3. a) Experimental compression test, b) numerical compression test, c) experimental Brazilian test, and d) numerical Brazilian test.

Table 1. Micro-parameters of rock sample.

Micro-parameters	Value	Micro-parameters	Value
Disc radius ratio	1.76	Parallel bond normal strength (MPa)	$10 \pm 2$
Disc density ( $\text{kg}\cdot\text{m}^{-3}$ )	2500	Parallel bond shear strength (MPa)	$10 \pm 2$
Disc contact modulus (GPa)	3.5	Parallel bond stiffness ratio	1.5
Parallel bond modulus (GPa)	3.5	Parallel bond radius multiplier	1
Disc stiffness ratio	1	Minimum radius (mm)	0.27
Disc friction coefficient	0.5		

Table 2. Mechanical properties in numerical models.

Parameters	Numerical output	Experimental result
Uniaxial compressive strength (MPa)	7.4	7.2
Young modulus (GPa)	9.3	9.1
Tensile strength (MPa)	1.4	1.3

### 2.2.2. Simulation of Rock Bolt

The bolt is represented by a cluster of balls with parallel bonds that meet the requirements of the force-displacement law. The parallel bond transmits both the forces and the moments between disks, which is consistent with the stress state in a bolt. The micro-parameters of the bolt are determined via the bolt pull-out test, as shown in

Figure 4a. The micro-parameters of the bolt are shown in Table 3. Figure 4b describes the stress-strain obtained by the pull out test. When the magnitude of the axial stress in the bolt exceeds the maximum normal stress, the bonds are broken, and the bolt will lose its bearing capacity. The tensile strength of the simulated rock bolt was 360 MPa. It was assumed that the bond failure occurred in the rock bolt.

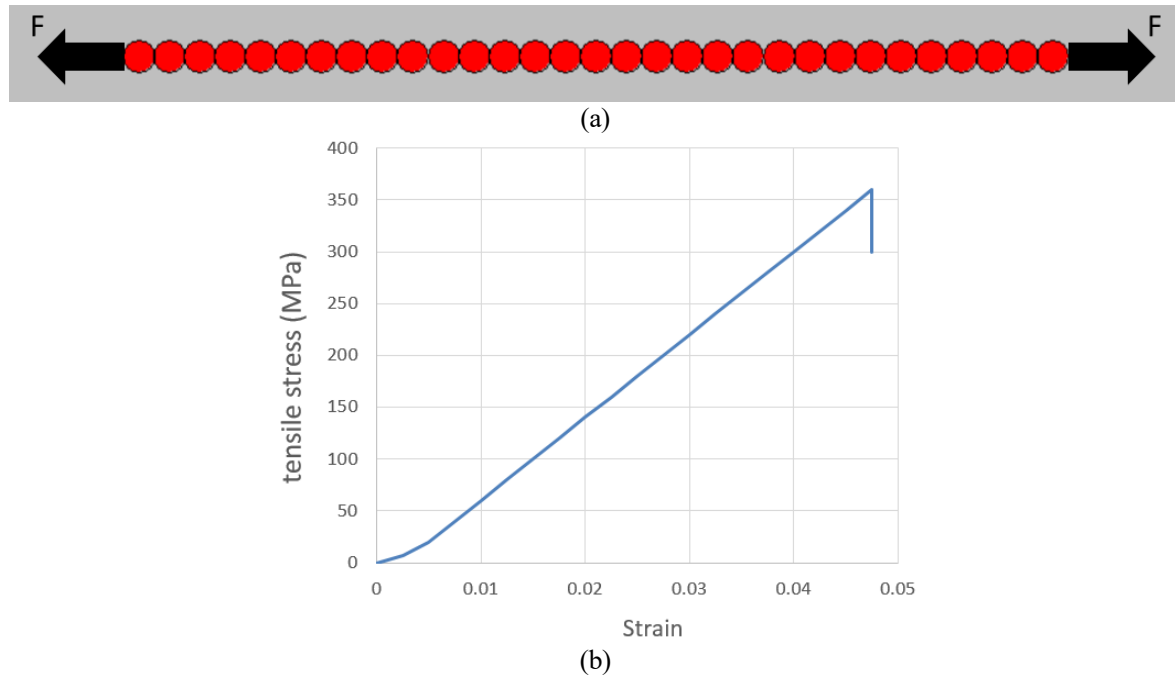


Figure 4. a) Rock bolt under tensile load, b) tensile stress versus strain for rock bolt.

Table 3. Micro-parameters of rock bolt.

Micro-parameters	Value	Micro-parameters	Value
Disc radius (mm)	1	Parallel bond normal strength (MPa)	$350 \pm 20$
Disc density ( $\text{kg.m}^{-3}$ )	7500	Parallel bond shear strength (MPa)	$250 \pm 20$
Disc contact modulus (GPa)	35	Parallel bond stiffness ratio	2.5
Disc stiffness ratio	1.3	Parallel bond radius multiplier	1
Disc friction coefficient	7	Parallel modulus (GPa)	35

### 2.3. Direct Shear Test Model of Bolted Joint

The direct shear test model was built using PFC2D (Figures 5). The PFC specimen had the dimensions of  $100 \text{ mm} \times 100 \text{ mm}$ . A total of 13268 disks with a minimum radius of 0.27 mm were used to make up the box specimen. Four walls existed at the upper, lower, left, and right sides of the model. The shear test condition was created by deletion of two narrow bands of particle from the upper and lower parts of the model (Figures 5-7). The non-persistent joints were formed by deletion of bands of particles from the model. The opening of these notches was 1 mm (Figures 5-7). The model and rock bolts were specified by the blue and green

color, respectively. The joint lengths were 7 cm, 5 cm, and 3 cm (Figures 5-7). The rock bolt length was 5 cm, and its angles related to horizontal axis were  $0^\circ$ ,  $15^\circ$ ,  $30^\circ$ ,  $45^\circ$ ,  $60^\circ$ , and  $75^\circ$  (Figures 5-7). Totally, 18 different models were prepared for numerical simulation. The upper and lower walls applied shear force on the model. The shear force was registered by taking the reaction forces on the upper wall (Figures 5-7). Also the shear displacement was registered by movement of the upper wall (Figures 5-7). The left and right walls applied normal forces on the model (Figures 5-7). In this work, the normal stress applied in the shear surface was 2 MPa.

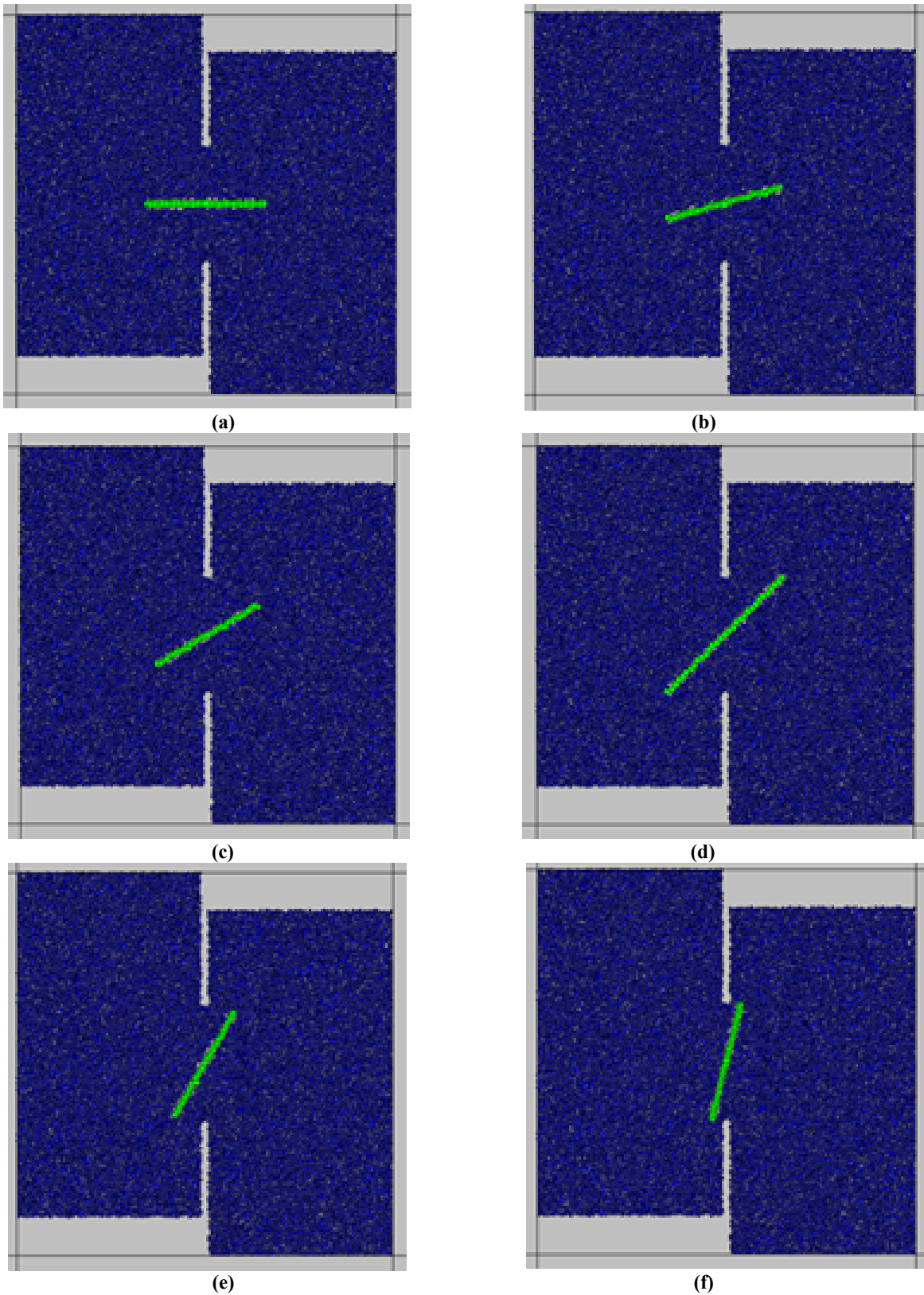


Figure 5. Numerical model with a Rock Bridge length of 3 cm and rock bolt angles of a. 0°, b. 15°, c. 30°, d. 45°, e. 60°, and f. 75°.

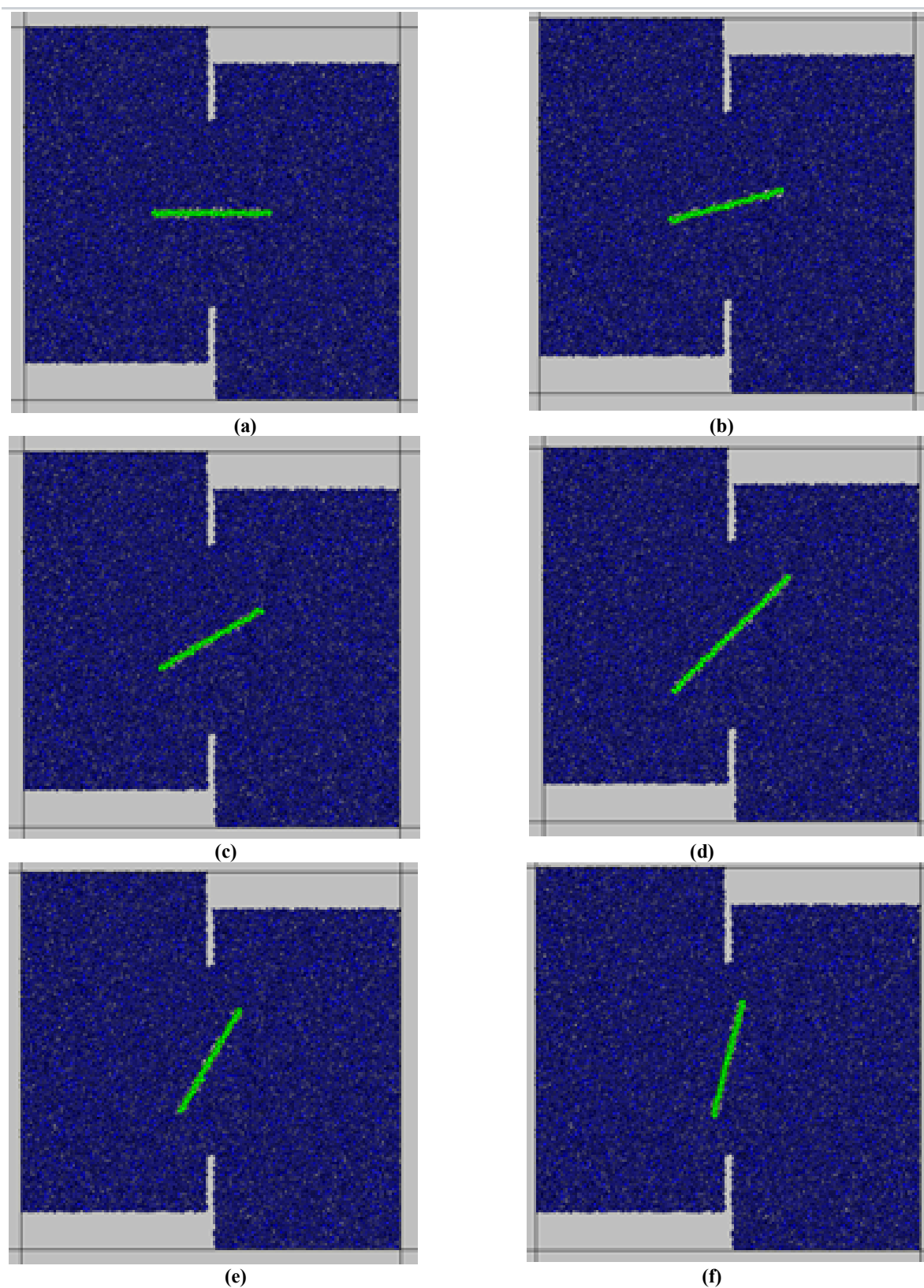


Figure 6. Numerical model with a Rock Bridge length of 5 cm and rock bolt angles of a. 0°, b. 15°, c. 30°, d. 45°, e. 60°, and f. 75°.

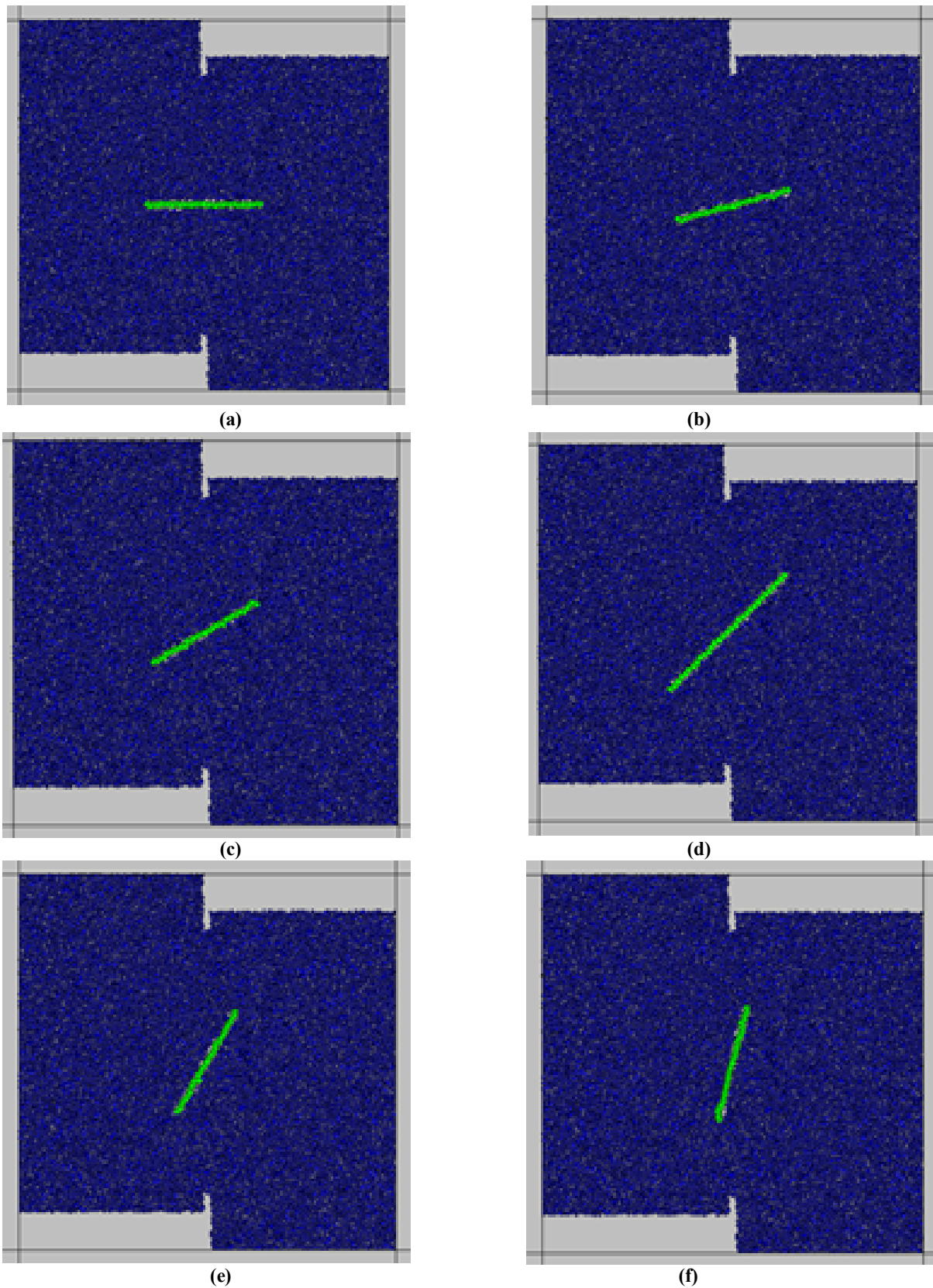


Figure 7. Numerical model with a Rock Bridge length of 7 cm and rock bolt angles of a. 0°, b. 15°, c. 30°, d. 45°, e. 60°, and f. 75°.

### 3. Numerical results

#### 3.1. Effect of Rock Bridge length and rock bolt angle on failure pattern of numerical model

Figures 8-10 show the effect of the Rock Bridge length and rock bolt angle on the failure pattern of the numerical model.

a) Rock Bridge length was 3 cm:

When the rock bolt angle was  $0^\circ$  (Figures 8a), firstly, two tensile cracks initiated from the rock bolt and propagated toward the joint tip. Also two tensile cracks initiated from the joint tips and propagated parallel to the loading axis till coalescence with the rock bolt. This trend was similar for other rock bolt angles, i.e.  $15^\circ$  (Figures 8b),  $30^\circ$  (Figures 8c),  $45^\circ$  (Figures 8d),  $60^\circ$  (Figures 8e), and  $75^\circ$  (Figures 8f).

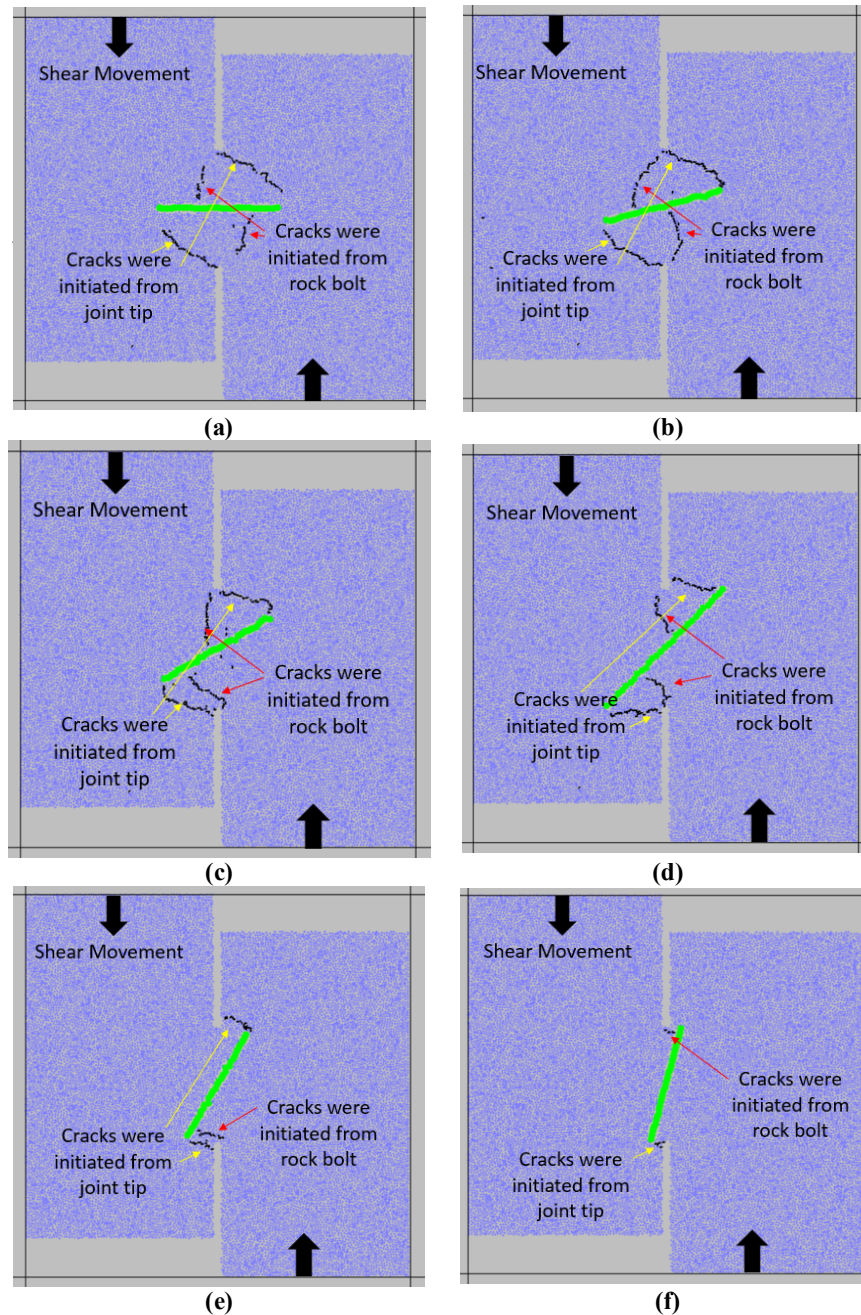


Figure 8. Numerical model with a Rock Bridge length of 3 cm and rock bolt angles of a)  $0^\circ$ , b)  $15^\circ$ , c)  $30^\circ$ , d)  $45^\circ$ , e)  $60^\circ$ , and f)  $75^\circ$ .

b) Rock Bridge length was 5 cm:

When the rock bolt angle was  $0^\circ$  (Figures 9a), firstly, two tensile cracks initiated from the rock bolt and propagated toward the joint tip. Also two tensile cracks initiated from the joint tips and

propagated parallel to the loading axis till coalescence with the rock bolt. This trend was similar for the other rock bolts angles, i.e.  $15^\circ$  (Figures 9b),  $30^\circ$  (Figures 9c),  $45^\circ$  (Figures 9d),  $60^\circ$  (Figures 9e), and  $75^\circ$  (Figures 9f).

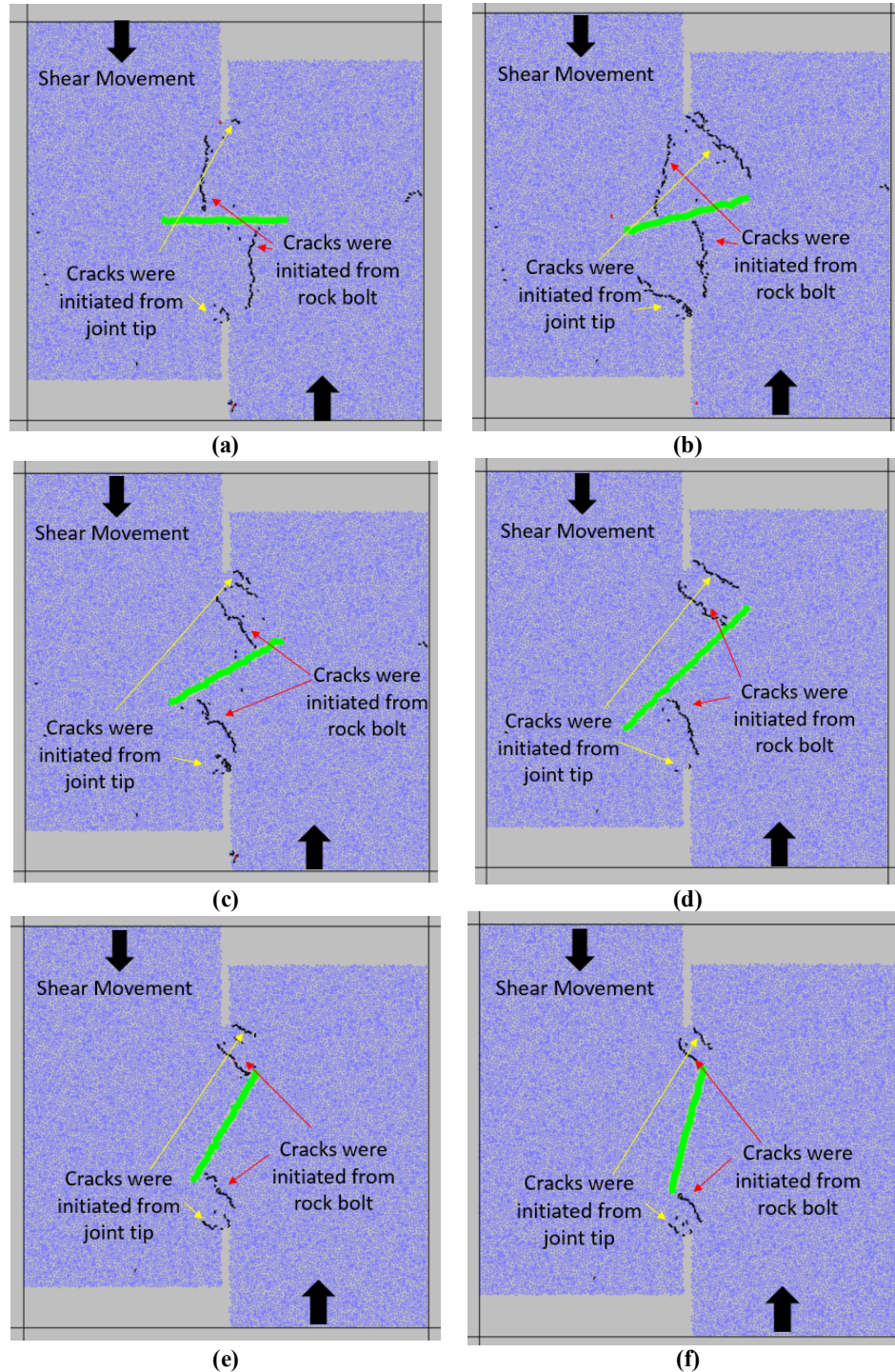


Figure 9. Numerical model with a Rock Bridge length of 5 cm and rock bolt angles of a)  $0^\circ$ , b)  $15^\circ$ , c)  $30^\circ$ , d)  $45^\circ$ , e)  $60^\circ$ , and f)  $75^\circ$ .

c) Rock Bridge length was 7 cm:

When the rock bolt angle was  $0^\circ$  (Figures 10a), firstly, two tensile cracks initiated from the rock bolt and propagated toward the joint tip. Also two tensile cracks initiated from the joint tips and

propagated parallel to the loading axis till coalescence with the rock bolt. This trend was similar for other rock bolt angles, i.e.  $15^\circ$  (Figures 10b),  $30^\circ$  (Figures 10c),  $45^\circ$  (Figures 10d),  $60^\circ$  (Figures 10e), and  $75^\circ$  (Figures 10f).

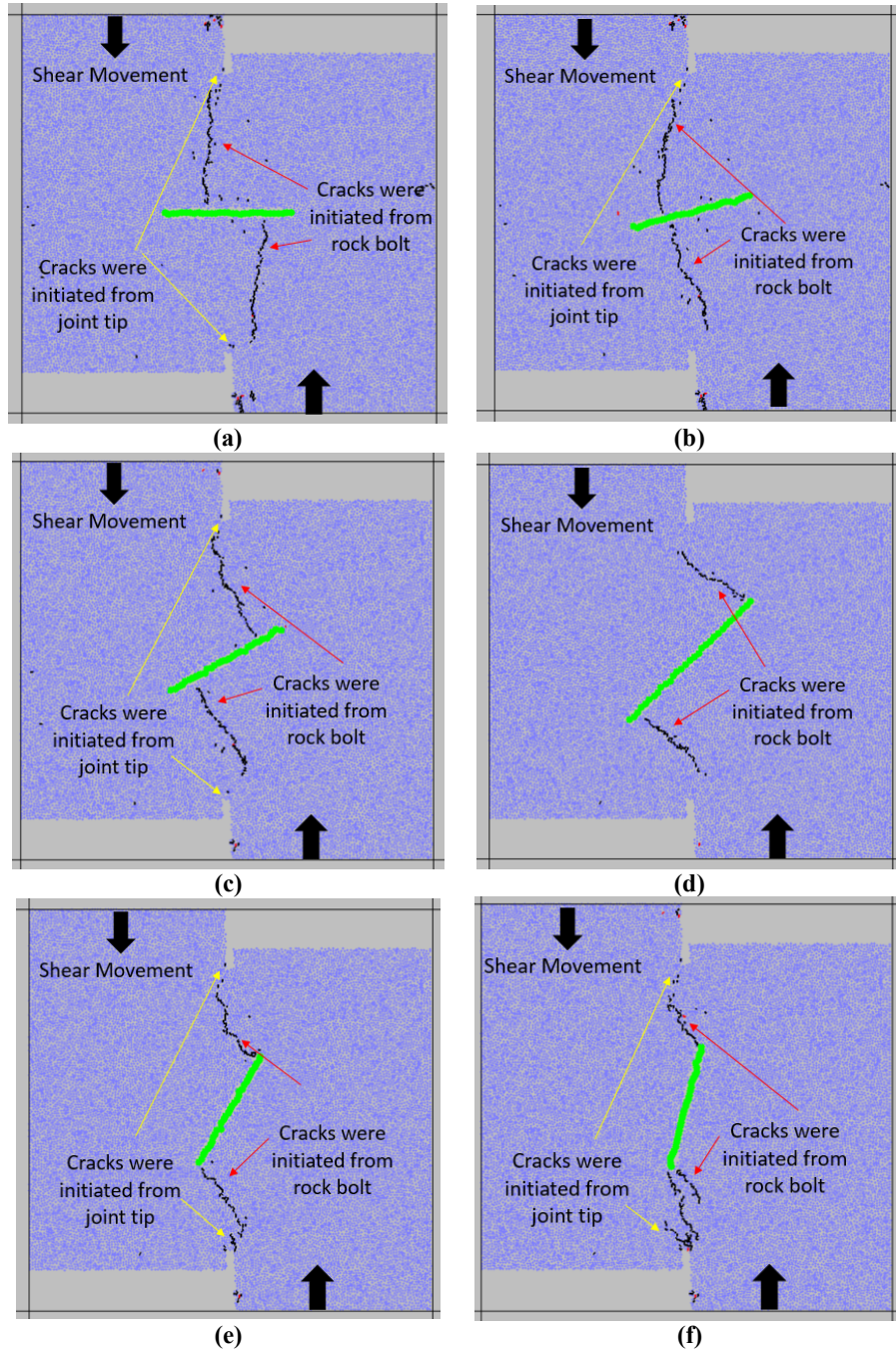


Figure 10. Numerical model with a Rock Bridge length of 7 cm and rock bolt angles of; a)  $0^\circ$ , b)  $15^\circ$ , c)  $30^\circ$ , d)  $45^\circ$ , e)  $60^\circ$ , and f)  $75^\circ$ .

### 3.2. Effect of rock bolt angle on shear strength of numerical model

Figure 11 shows the effect of the rock bolt angle on the shear strength of the numerical model. The meaning of shear strength is division of the final failure load by the total failure surface that is 100 mm. The results of three Rock Bridge lengths are depicted in this figure. The shear strength was decreased by increasing the rock bolt angle. This trend was similar for different Rock Bridge lengths or connected areas.

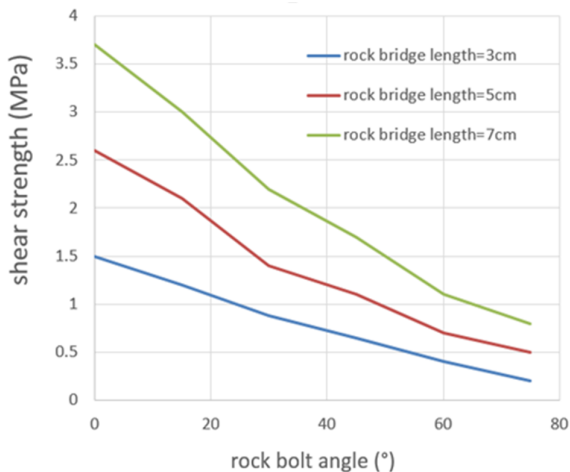


Figure 11. Effect of rock bolt angle on shear strength of numerical model. This is an unusual report, and is not the real case in the field.

### 3.4. Bond force distribution before crack initiation for rock bolt angle of 90°

Figure 13 shows the illustration of the bond force distribution before the crack initiation for the rock bolt angle of 90°. The red and black lines are representative of the tensile force and compressive force, respectively. The bond force is initially concentrated on the joint. The value of the maximum tensile force before crack initiation for the Rock Bridge lengths of 3 cm, 5 cm, and 7 cm were  $4 \times 10^4$  N,  $5.3 \times 10^4$  N, and  $6.2 \times 10^4$  N, respectively. As the shear displacement increases, the disk's contact force around the bolt becomes gradually larger. In addition, the distribution of

### 3.3. Effect of rock bolt angle on maximum shear displacement

Figure 12 shows the effect of the rock bolt angle on the maximum shear displacement of numerical model. The results of three Rock Bridge lengths are depicted in this figure. The maximum shear displacement was decreased by increasing the rock bolt angle. This trend was similar for different Rock Bridge lengths.

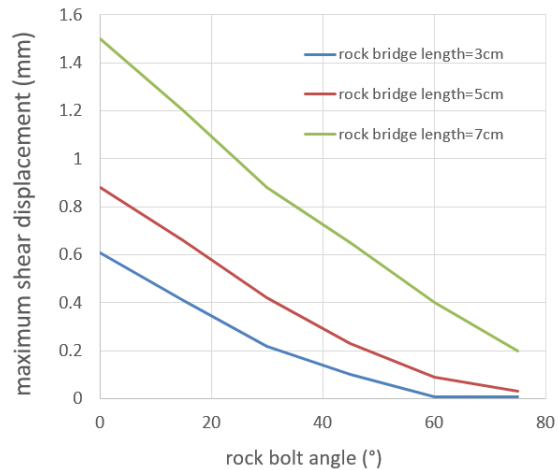


Figure 12. Effect of the rock bolt angle on shear strength of the numerical model.

cracks corresponds to the contact force in the stress concentration area.

## 4. Discussion

From the above findings, it could be concluded that when the rock bolt angle was 90°, the shear strength had a maximum value. In fact, in this configuration, the tensile crack propagation length had a maximum value. By increasing the rock bolt angle, the length of the connected area was decreased so the shear strength was decreased. The failure pattern was similar by increasing the rock bridge length and the rock bolt angle.

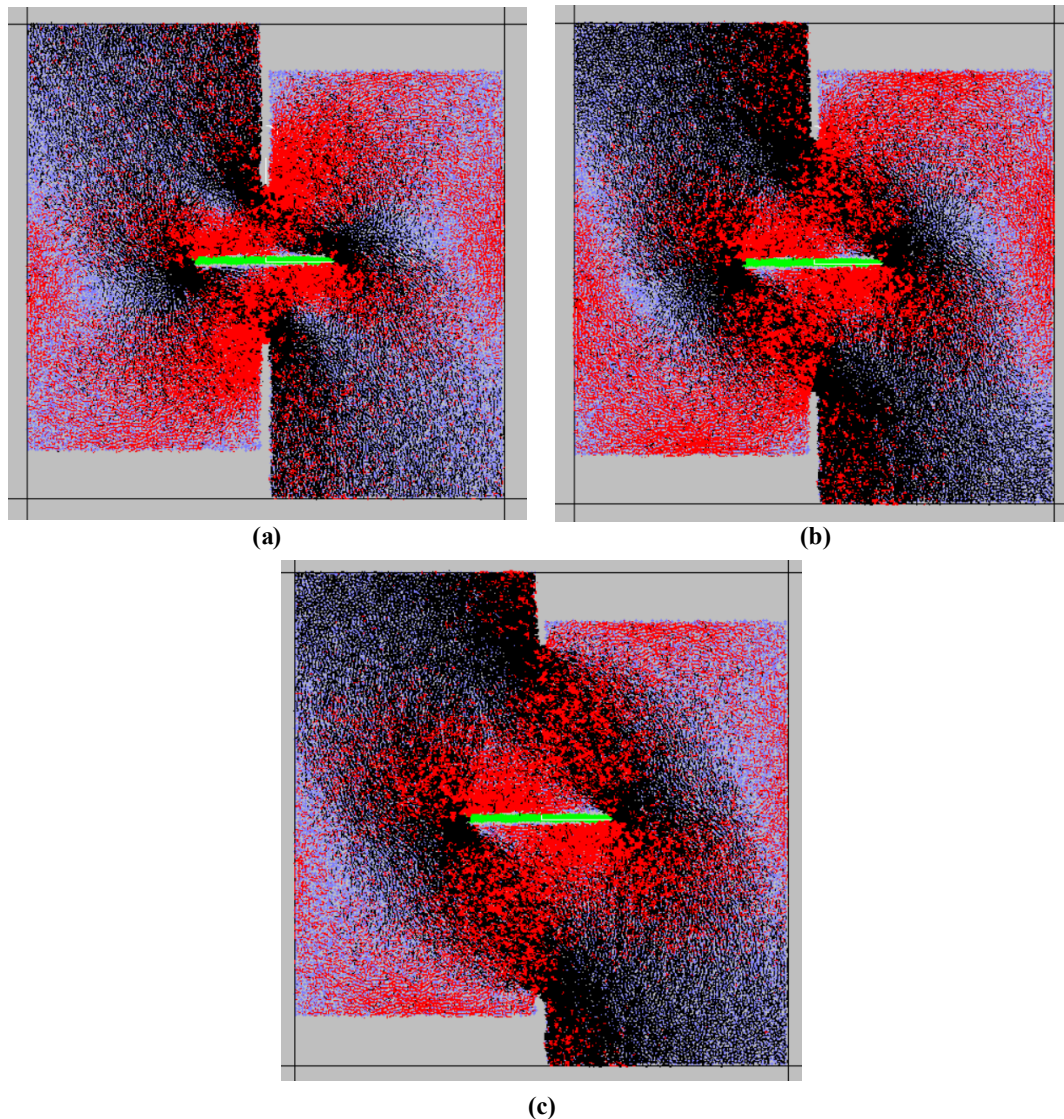


Figure 13. Bond force distribution before crack initiation for the rock bolt angle of  $90^\circ$  and the Rock Bridge lengths of a) 3 cm, b) 5 cm, and c) 7 cm. How much is the value of the tensile force before crack initiation?

## 5. Conclusions

In this work, the effect of the rock bolt angle on the shear behavior of Rock Bridges was investigated using the particle flow code in two dimensions (PFC2D). Firstly, the calibration of PF2D was performed to reproduce the gypsum sample. Then the numerical models with the dimensions of  $100 \text{ mm} \times 100 \text{ mm}$  were prepared. The Rock Bridge was created in the middle of the model by removal of the narrow bands of discs from it. The Rock Bridge lengths were 30 mm, 50 mm, and 70 mm. The rock bolt was calibrated by a parallel bond. One rock bolt was inserted into the Rock Bridge. The rock bolt angles related to the horizontal axis were changed from  $0^\circ$  to  $75^\circ$ . Totally, 18 models were prepared. The shear test

condition was added to the models. The normal load was fixed at 3 MPa ( $\sigma_c/3$ ), and the shear load was added to the model till failure occurred. The results obtained shows making a model with the same size but without bolts, and report the results and put them beside the results and compare the with the bolt case.

- When the rock bolt angle was  $0^\circ$ , firstly, two tensile cracks initiated from the rock bolt and propagated toward the joint tip. Also two tensile cracks initiated from the joint tips and propagated parallel to the loading axis till coalescence with the rock bolt. This trend was similar for the other rock bolts angles. Also this trend was similar for three different Rock Bridge lengths.

- The shear strength was decreased by increasing the rock bolt angle. This trend was similar for different Rock Bridge lengths.
- The maximum shear displacement was decreased by increasing the rock bolt angle. This trend was similar for different rock bridge lengths.
- The bond force was initially concentrated on the joint. As the shear displacement increased, the disk's contact force around the bolt became gradually larger. In addition, the distribution of cracks corresponds to the contact force in the stress concentration area.
- The authors suggest to study the shear behavior of the echelon joints in the presence of rock bolts.

## References

- [1]. F. D. Patton, "Multiple modes of shear failure in rock," in Proceedings of the 1<sup>st</sup> Congress on International Society for Rock Mechanics, pp. 509–513, 1966.
- [2]. R. E. Goodman, Methods of Geological Engineering in Discontinuous Rocks, West Publishing Company, New York, NY, USA, 1976.
- [3]. N. Barton and V. Choubey, "The shear strength of rock joints in theory and practice," Rock Mechanics, Vol. 10, No. 1-2, pp. 1–54, 1977.
- [4]. P. M. Dight and H. K. Chiu, "Prediction of shear behavior of joints using profiles," International Journal of Rock Mechanics and Mining Sciences & Geomechanics Abstracts, Vol. 18, No. 5, pp. 369–386, 1981.
- [5]. N. Barton, Modelling Rock Joint Behaviour from *in situ* Block Tests: Implications for Nuclear Waste Repository Design, Vol. 308, Office of Nuclear Waste Isolation, ONWI, Columbus, OH, USA, 1982.
- [6]. T. Esaki, S. Du, Y. Jiang, and Y. Wada, "Effect of the asperity damage on the shear behavior of irregular rock joints," in Proceedings of the Second International Conference on Analysis of Discontinuous Deformation, pp. 459–464, Kyoto, Japan, 1997.
- [7]. Y. Jiang, J. Xiao, Y. Tanabashi, and T. Mizokami, "Development of an automated servo-controlled direct shear apparatus applying a constant normal stiffness condition," International Journal of Rock Mechanics and Mining Sciences, Vol. 41, No. 2, pp. 275–286, 2004.
- [8]. Y. J. Jiang, B. Li, and Y. Tanabashi, "Estimating the relation between surface roughness and mechanical properties of rock joints," International Journal of Rock Mechanics and Mining Sciences, Vol. 43, No. 6, pp. 837–846, 2006.
- [9]. C. C., Xia, Z. C. Tang, W. M. Xiao, and Y. L. Song, "New peak shear strength criterion of rock joints based on quantified surface description," Rock Mechanics and Rock Engineering, Vol. 47, No. 2, pp. 387–400, 2014.
- [10]. S. Bjurström, "Shear strength of hard rock joints reinforced by grouted untensioned bolts," in Proceedings of the In Proceedings of the 3rd International ISRM Congress, pp. 1194–1199, Denver, Colo, USA, 1974.
- [11]. X. Ge and J. Liu, "Study of the shear resistance behavior of bolted rock joints," Journal of Geotechnical Engineering, Vol. 10, No. 1, pp. 8–19, 1988 (Chinese).
- [12]. K. Spangand, P. Egger, "Action of fully-grouted bolts in jointed rock and factors of influence," Rock Mechanics and Rock Engineering, Vol. 23, No. 3, pp. 201–229, 1990.
- [13]. P. Egger and L. Zabuski, "Behaviour of rough bolted joints in direct shear tests," in Proceedings of the 7<sup>th</sup> ISRM Congress, Vol. 30, p. Aachen, Germany, September 1991.
- [14]. A. M. Ferrero, "The shear strength of reinforced rock joints," International Journal of Rock Mechanics and Mining Sciences, Vol. 32, No. 6, pp. 595–605, 1995.
- [15]. F. Pellet and P. Egger, "Analytical model for the mechanical behavior of bolted rock joints subjected to shearing," Rock Mechanics and Rock Engineering, Vol. 29, No. 2, pp. 73–97, 1996.
- [16]. H. Jalalifar and N. Aziz, "Experimental and 3D numerical simulation of reinforced shear joints," Rock Mechanics and Rock Engineering, Vol. 43, No. 1, pp. 95–103, 2010.
- [17]. P. Wang, T. Feng, Y. J. Zhu, and W. J. Yu, "Experimental study and numerical simulation of anchoring mechanism of anchored rock like material with prefabricated fracture," Yantu Lixue/Rock and Soil Mechanics, Vol. 37, No. 3, pp. 793–801, 2016 (Chinese).
- [18]. L. Li, P. C., S. Saydam, B. Hebblewhite, and Y. Li, "Parametric study of rock bolt shear behavior by double shear test," Rock Mechanics and Rock Engineering, Vol. 49, No. 12, pp. 4787–4797, 2016.
- [19]. Itasca Consulting Group Inc., "PFC2D (Particle Flow Code in 2D) Theory and Background," Minneapolis, Minn, USA, 2008.
- [20]. P. A. Cundall and O. D. L. Strack, "The distinct numerical model for granular assemblies," Geotechnique, Vol. 29, No. 1, pp. 47–65, 1979.
- [21]. J. Zhou and Y. Chi, "The method of particle flow and PFC2D code," Rock and Soil Mechanics, Vol. 21, No. 3, pp. 271–274, 2000 (Chinese).

- [21]. D. O. Potyondy and P. A. Cundall, "A bonded-particle model for rock," *International Journal of Rock Mechanics and Mining Sciences*, Vol. 41, No. 8, pp.1329–1364, 2004.
- [22]. N. Cho, C.D. Martin, and D.C.S ego, "A clumped particle model for rock," *International Journal of Rock Mechanics and Mining Sciences*, Vol. 44, No. 7, pp. 997–1010, 2007.
- [23]. Z. Zhao, L. Jing and I. Neretnieks, "Particle mechanics model for the effects of shear on solute retardation coefficient in rock fractures," *International Journal of Rock Mechanics and Mining Sciences*, Vol. 52, pp. 92–102, 2012.
- [24]. C. Xia, Y. Song, Z. Tang, Y. Song, and C. Shou, "Particle flow numerical simulation for shear behavior of rough joints," *Chinese Journal of Rock Mechanics and Engineering*, Vol. 31, No. 8, pp. 1545–1552, 2012 (Chinese).
- [25]. Y. Zhou, A. Misra, S. Wu, and X. Zhang, "Macro- and meso-analyses of rock joint direct shear test using particle flow theory," *Chinese Journal of Rock Mechanics and Engineering*, Vol. 31, No. 6, pp. 1245–1256, 2012.
- [26]. R.H. Cao, P. Cao, H. Lin, K. Zhang, and X.W. Tan, "Particle flow analysis of direct shear tests on joints with different roughness," *Rock and Soil Mechanics*, Vol. 34, supplement 2, pp. 456–464, 2013 (Chinese).
- [27]. Ghazvinian, A., Sarfarazi, V., Schubert, W., and Blumel, M. (2012), "A study of the failure mechanism of planar non-persistent open joints using PFC2D", *Rock Mech. Rock Eng.*, 45(5), 677-693.

## مطالعه عددی تاثیر زاویه داری راک بولت بر رفتار برشی پل سنگ

وهاب سرفرازی<sup>۱\*</sup> و عبدالله تبریی<sup>۲</sup>

۱- گروه مهندسی معدن، دانشگاه صنعتی همدان، همدان، ایران  
۲- گروه مهندسی عمران، موسسه آموزش عالی اشراق، بجنورد، ایران

ارسال ۲۰۲۰/۰۴/۱۸، پذیرش ۲۰۲۰/۱۰/۰۱

\* نویسنده مسئول مکاتبات: sarfarazi@hut.ac.ir

## چکیده:

در این مقاله تاثیر زاویه داری راک بولت بر رفتار برشی پل سنگ با سه طول مختلف تو سط نرم افزار PFC مطالعه شده است. در ابتدا نرم افزار برای نمونه گچ کالیبره گردید. سپس مدل عددی با ابعاد  $100 \text{ mm} \times 100 \text{ mm}$  آماده شد. پل سنگ در مرکز مدل با حذف نوارهایی از دیسک‌ها ایجاد شد. مقاومت تک محوره پل سنگ  $17/4 \text{ MPa}$  است. طول پل سنگ در سه مقدار  $30 \text{ mm}$ ،  $50 \text{ mm}$  و  $70 \text{ mm}$  متغیر است. راک بولت با اتصال موازی کالیبره شد. مقاومت کششی راک بولت  $1360 \text{ MPa}$  است. یک راک بولت در پل سنگ نصب گردید. زاویه داری راک بولت با افق از صفر تا  $75^\circ$  درجه با گام‌های  $15^\circ$  درجه تغییر می‌کند. بطور کلی  $18$  مدل آماده سازی شد. شرایط برش مستقیم برای مدل‌ها مهیا شد. تنش نرمال  $2 \text{ MPa}$  به مدل‌ها اعمال گردید و بار برشی تا لحظه شکست به مدل‌ها اعمال گردید. نتایج نشان می‌دهند که در زاویه داری ثابت راک بولت، ترک‌های کششی از نوک درزه شروع شده، به موازات محور بارگذاری برشی رشد کرده و به راک بولت متصل می‌گردد. در طول ثابت پل سنگ، مقاومت برشی با افزایش زاویه داری راک بولت افزایش می‌یابد. بیشترین مقاومت برشی در زاویه داری صفر درجه اتفاق می‌افتد.

کلمات کلیدی: راک بولت، پل سنگ، PFC2D.